AJNR

0.6 T Magnetic Resonance Imaging of the Orbit

Jon H. Edwards, Roger A. Hyman, S. J. Vacirca, Michael A. Boxer, Samuel Packer, Ira H. Kaufman and Harry L. Stein

AJNR Am J Neuroradiol 1985, 6 (2) 253-258
http://www.ajnr.org/content/6/2/253

0.6 T Magnetic Resonance Imaging of the Orbit

Jon H. Edwards[1]
Roger A. Hyman[1]
S. J. Vacirca[1]
Michael A. Boxer[2]
Samuel Packer[2]
Ira H. Kaufman[2]
Harry L. Stein[1]

Magnetic resonance (MR) imaging of the orbit was performed with a 0.6 T superconducting imaging system in 100 patients with normal orbits who were being evaluated for brain pathology and in 21 additional patients with a variety of orbital lesions to determine the efficacy of MR imaging in displaying orbital abnormalities. Usually, MR studies were performed using a multislice technique with multiple spin-echo pulse sequences and 30, 60, and 90 msec echo times and 500, 1500, and 2000 msec repetition times. Using section thicknesses of about 8 mm, imaging was performed in the transaxial, coronal, and sagittal projections. Pixel size was 0.9 × 1.8 mm, and the examination took about 30 min. The MR findings were compared with computed tomographic (CT) findings in all cases. Either combined axial and coronal studies of 5-mm-thick sections or a thin axial study of 1-mm-thick sections followed by reformatting techniques to obtain multiplanar images was used. Contrast enhancement was used in the CT studies. Both MR and CT clearly demonstrated the soft-tissue abnormality in all cases except two, in which MR failed to detect the abnormality. In one, MR failed to detect a small retrobulbar hemorrhage that occurred after a surgical procedure for retinal detachment. In the second case, rather extensive calcification in the posterior choroidal layers and lens was not detected by MR imaging. In several other cases, MR provided information beyond that obtained with CT. MR has the advantage of providing exquisite anatomic detail in multiplanar images, and it appears to be more sensitive than CT in detecting small, subacute and chronic hemorrhage within soft-tissue masses in the orbit and in detecting ischemia of the globe. CT is superior to MR imaging in portraying fine bone detail.

Application of magnetic resonance (MR) imaging to the orbit is attractive because multiplanar techniques can be performed without additional positioning and the risks of ionizing radiation and contrast administration are eliminated. Compared with computed tomography (CT), MR appears particularly advantageous in providing excellent anatomic detail of the intracranial part of the optic nerve and chiasm in the sagittal plane and provides information concerning its alteration by pathologic masses. We evaluated MR images of the orbits in 21 patients with known orbital lesions to determine its clinical efficacy.

Subjects and Methods

We evaluated the MR images of the orbits in 100 patients who were being examined for brain pathology. Twenty-one additional patients with known orbital lesions were evaluated with MR. Sixteen tumorous conditions involving the orbits, four cases of inflammatory lesions, and one retrobulbar hemorrhage were examined (table 1). Four patients had space-occupying lesions of the globe and 17 had extraocular masses involving the orbit. Age range of the patients was 21–84 years.

Our findings were correlated with surgical and pathologic findings and, in some cases of inflammatory disease, with response to medical therapy. The MR images were compared with CT scans. A CT study of each patient was performed with a Picker 1200 scanner using either combined axial and coronal studies of 5 mm section thickness or a thin axial study of

This article appears in the March/April 1985 issue of *AJNR* and the May 1985 issue of *AJR*.

Received July 25, 1984; accepted after revision October 10, 1984.

Presented at the annual meeting of the American Society of Neuroradiology, Boston, June 1984.

[1] Department of Radiology, Cornell University Medical College, New York, NY 10021, and North Shore University Hospital, 300 Community Dr., Manhasset, NY 11030. Address reprint requests to J. H. Edwards.

[2] Ophthalmology, Cornell University Medical College, New York, NY 10021, and North Shore University Hospital, Manhasset, NY 11030.

***AJNR* 6:253–258, March/April 1985**
0195–6108/85/0602–0253

1 mm sections followed by reformatting techniques to obtain multiplanar images. MR was performed on a 0.6 T superconducting imaging system (Technicare, Solon, OH). The principles underlying pulse sequences and the technique of MR imaging have been described [1–4]. In most cases, the examination was performed using multislice technique with multiple spin-echo (SE) pulse sequences with echo times (TEs) of 30, 60, and 90 msec and repetition times (TRs) of 500, 1500, and 2000 msec. In all cases imaging was performed in transaxial, coronal, and sagittal projections. With this technique the section thickness of each image plane was about 8 mm. The pixel size was 0.9 mm in the *x* axis and 1.8 mm in the *y* axis. Generally, complete examination was performed in about 30 min.

Results

In our experience the SE 500/30 pulse sequence with multislice technique afforded optimal contrast between pathologic masses and normal anatomic structures and allowed good spatial resolution with a high signal-to-noise (S/N) ratio. The longer T2-weighted SE pulse sequences provided increased spatial blurring with a less favorable S/N ratio; and contrast between pathologic masses and normal tissue was lost in many cases, so that the pathologic mass was undetected. As shown in a case of an intraocular melanoma (fig. 1), the tumor mass was demonstrated best on the T1-weighted pulse sequence where the tumor had a short T1 relative to the adjacent vitreous, providing sharp contrast and good anatomic definition. However, on the T2-weighted pulse sequence, as the signal intensity from the vitreous increased due to its long T2, contrast between the tumor and the vitreous was less, and the tumor was not as readily visible.

TABLE 1: **Pathologic Lesions in Patients with Known Orbital Lesions Who Were Evaluated by MR Imaging**

Type of Lesion	No. of Cases
Tumor:	
Optic nerve glioma	1
Optic nerve meningioma	1
Lymphoma	2
Melanoma	4
Metastasis	2
Meningioma	3
Direct extension from paranasal sinuses by mucoepidermoid carcinoma (1), squamous-cell carcinoma (1), and ossifying fibroma (1)	3
Subtotal	16
Inflammatory	4
Hemorrhagic	1
Total	21

Of the 21 lesions studied with both MR and CT, MR failed to detect the abnormality in only two cases. In the first, a small retrobulbar hemorrhage on the right (fig. 2) followed a surgical procedure for retinal detachment. Because of the high-signal retrobulbar fat, contrast between the high-signal small hemorrhage and fat was not sufficient to detect the abnormality. The second patient demonstrated rather extensive calcification in the posterior choroidal layers and lens of the left eye that was not detected on the MR image. In the other 19 cases, both MR and CT detected the soft-tissue abnormality. In many cases, additional information was provided by MR. In a case of Kimura disease of the orbit (fig. 3), which is a highly vascular inflammatory condition characterized pathologically by angiolymphoid hyperplasia [5], MR demonstrated areas of increased signal within a large soft-tissue mass, indicating areas of hemorrhage into the mass, pathologically proven to be subacute and chronic hemorrhage. CT demonstrated merely a homogeneously dense mass in which the areas of hemorrhage were not detected. In a case of devitalization of the left globe (fig. 4), signal intensity from both the vitreous and choroidal layers of the devitalized globe was dramatically different from the normal globe, and CT failed to demonstrate any asymmetry in appearance of the globes. Pathologically, the vitreous had undergone liquefaction accounting for its prolonged T2. In a case of ossifying fibroma of the sphenoid sinus, both MR and CT demonstrated a large soft-tissue mass filling the sphenoid sinus, eroding through the floor of the anterior cranial fossa. MR demonstrated the tumor to have long T1 and long T2 characteristics. Encroachment on the optic nerve by the tumor mass was seen well on the MR sagittal projection, where a change in signal intensity in the optic nerve was detected at the point of tumor involvement; this was not detected on CT. In our series of four melanomas, additional information was obtained with MR, although all were detected with both MR and CT. These tumors usually appeared to have relatively

Fig. 1.—Choroidal melanoma. SE 500/30 (**A**) and SE 2000/60 (**B**). Large tumor mass (t) occupies posterior part of left globe, which is optimally demonstrated on T1-weighted pulse sequence (**A**), where tumor has short T1 relative to adjacent vitreous, providing sharp contrast. However, on T2-weighted pulse sequence (**B**), contrast between tumor and vitreous is less, and tumor is not readily visible.

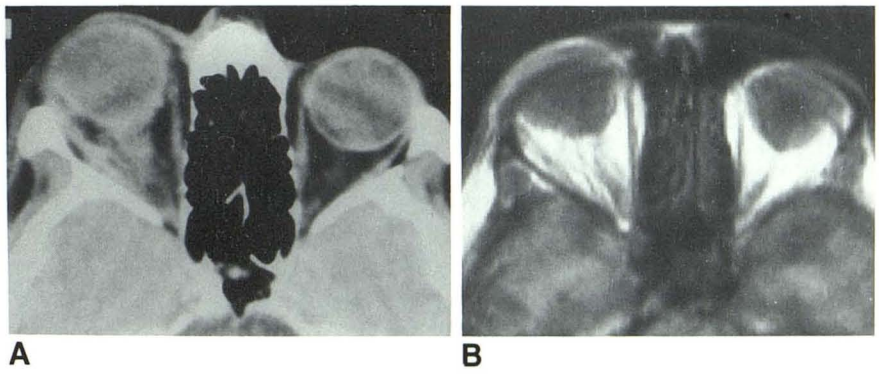

Fig. 2.—Retrobulbar hemorrhage. **A**, Contrast-enhanced CT scan. Small area of increased density represents hemorrhage in retrobulbar space. Associated proptosis of right globe. **B**, SE 500/30. Retrobulbar region appears slightly inhomogeneous, but hemorrhage is not definitely identified because contrast between high-signal small hemorrhage and high-signal fat was not sufficient to distinguish between the two.

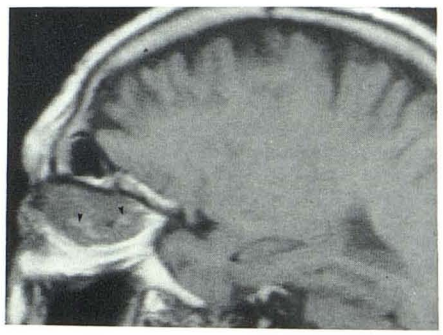

Fig. 3.—Kimura disease of orbit. Sagittal SE 500/30. Large soft-tissue mass occupies superior part of left orbit. Small areas of increased signal (*arrowheads*) indicate areas of hemorrhage into mass that were not detected on CT.

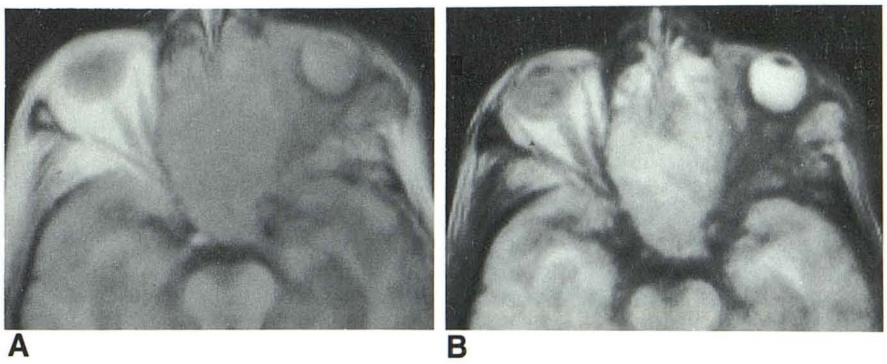

Fig. 4.—Devitalization of left globe. SE 500/30 (**A**) and SE 2000/90 (**B**). Signal intensity of vitreous of devitalized globe is markedly increased due to its prolonged T2, produced by liquefaction of the vitreous. Complete replacement of orbital fat on left and opacification of ethmoid air cells bilaterally by soft-tissue metastatic adenocarcinoma, which had resulted in ischemia of left globe.

high signal on the T1-weighted images, and increase in signal was noted in three of four of the melanomas on the T2-weighted images. These findings agree with those of DeLaPaz et al. [6] in MR of hemorrhagic lesions including melanomas. Since three of four melanomas showed a short T1 and long T2 (unlike the effect of a paramagnetic substance such as melanin, which would be expected to shorten both relaxation times), they appear to be comparable to other subacute or chronic hemorrhagic tissue in signal characteristics, with no clearly discernible paramagnetic effect of melanin. The one melanoma that demonstrated short T1 and short T2 most likely had these characteristics because of the paramagnetic effects of melanin. In all four melanomas, CT showed a nonenhancing hyperdense lesion that could have been interpreted as either tumor or hemorrhage. In a 4 mm melanoma (fig. 5) located in the medial quadrant of the left globe, both MR and CT detected the abnormality equally well, although the margins of the lesions were seen more clearly on CT.

Pathologic masses could be readily localized relative to and distinguished from the optic nerve, sometimes because of difference in signal intensity between the mass and the nerve; this was true for a large melanoma medial to the optic nerve (fig. 6). In other cases, masses could be distinguished from the optic nerve because of the detection of a layer of fat between the mass and nerve on the coronal or sagittal projection, which was not possible in the transaxial plane (fig. 7). Multislice technique in the sagittal projection consistently demonstrated excellent anatomic delineation of the 1.0–1.5-cm-long part of the intracranial optic nerve and optic chiasm (fig. 8). Imaging in the coronal and transaxial planes also consistently showed good visualization of the optic chiasm. When the chiasm was intrinsically involved with tumor, the extent of tumorous involvement was better appreciated by application of multiplanar imaging (fig. 9). A combination of transaxial, coronal, and sagittal projections clearly demonstrated the involvement of the intracranial optic nerve. Sagittal and coronal projections demonstrated the superior and inferior extent of the tumor, while involvement of the optic tracts posteriorly could be appreciated on the transaxial projection. MR sagittal projections also provided additional information concerning pathologic alteration of the optic nerve and chiasm by masses eroding through the floor of the anterior cranial fossa (fig. 10).

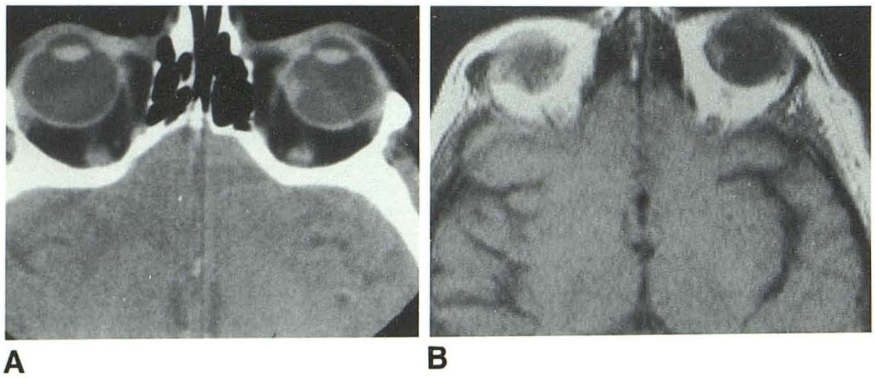

Fig. 5.—Choroidal melanoma. **A**, Contrast-enhanced CT scan shows 4 mm hyperdense lesion in medial quadrant of left globe that could represent either hemorrhage or tumor. Lesion had same appearance on unenhanced CT. **B**, SE 500/30. The 4 mm melanoma is well imaged in medial quadrant of left globe.

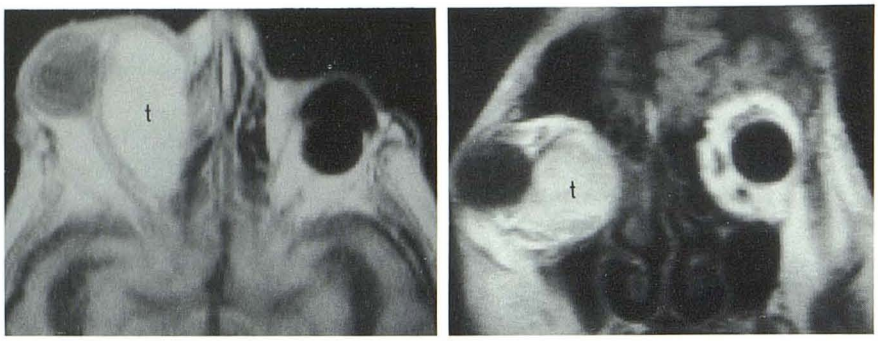

Fig. 6.—Metastatic melanoma. SE 500/30. **A**, Transaxial image. Large tumor mass (t) situated medial to right optic nerve and globe is well delineated and distinguished from adjacent optic nerve because of difference in signal intensity between mass and nerve. Melanoma is of high signal because of its short T1, most likely produced by hemorrhage into tumor. Optic nerve is very clearly delineated both from tumor mass and retroorbital fat lateral to nerve. Prosthetic device is in place in left orbit. **B**, Coronal image again demonstrates large high-signal tumor mass (t) in medial part of right globe, producing marked lateral deviation and proptosis of right globe. Medial rectus and inferior rectus muscles cannot be distinguished from this mass.

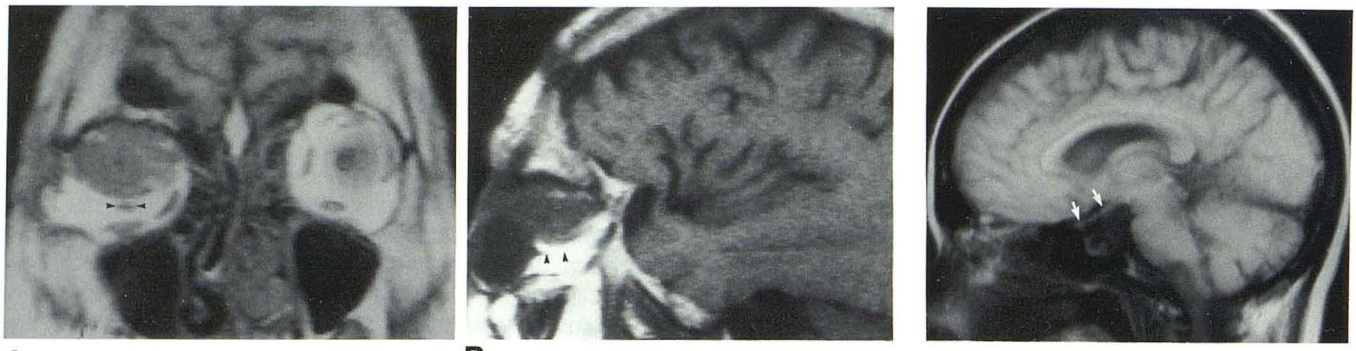

Fig. 7.—Orbital pseudotumor. SE 500/30. **A**, Coronal image. Good delineation of optic nerve (*arrowheads*) from large inflammatory mass superiorly by layer of high-signal fat between mass and nerve. **B**, Sagittal image. Good delineation of optic nerve (*arrowheads*) from large inflammatory mass separated by layer of high-signal fat.

Fig. 8.—Normal sagittal SE 500/30 image. Excellent anatomic delineation of intracranial part of optic nerve and optic chiasm. The 1.0–1.5-cm-long part of optic nerve (*arrows*) can be well seen in suprasellar region, forming optic chiasm posteriorly at junction of anterior wall and floor of third ventricle. Signal intensity of optic nerve and chiasm is similar to that of adjacent normal brain tissue, but is well defined because of good contrast with low-signal cerebrospinal fluid adjacent to it.

Discussion

CT is well known to be an effective and reliable means of examining the orbit [7–13]. Reports on the efficacy of MR in diagnosing cerebral and orbital abnormalities have been encouraging [14–21]. Application of MR to the orbit is attractive in that multiplanar techniques may be performed, providing additional information without additional positioning; and the

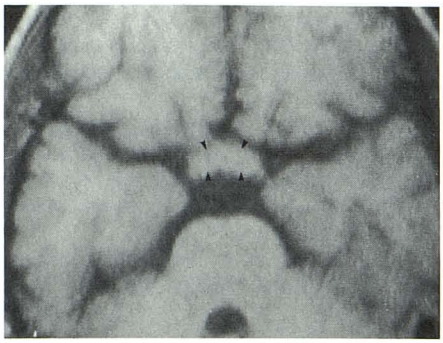

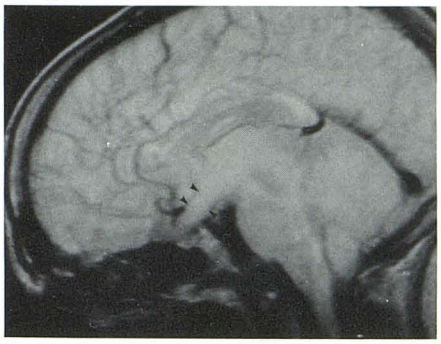

A B

Fig. 9.—Optic glioma. **A**, Transaxial SE 500/30 image. Good anatomic definition of optic chiasm (*arrowheads*), which is enlarged by tumor infiltration. Good contrast discrimination between optic chiasm and surrounding low-signal cerebrospinal fluid in suprasellar cistern. Optic tracts were seen well, and appeared normal on transaxial image just superior to this cut. **B**, Sagittal SE 2000/90 image. Extent of tumorous involvement of intracranial part of optic nerve and optic chiasm (*arrows*) is seen to good advantage, with markedly thickened and enlarged optic nerve and chiasm. Signal intensity of tumor is slightly increased due to prolonged T2.

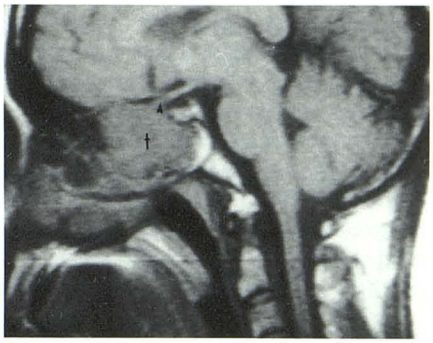

Fig. 10.—Extrinsic mass altering optic apparatus. Sagittal SE 500/30 image. Large tumor mass (t), pathologically confirmed as ossifying fibroma, fills sphenoid sinus, erodes through floor of anterior cranial fossa, and encroaches on optic nerve at point (*arrow-head*) just anterior and superior to sella turcica.

risks of ionizing radiation and contrast administration are eliminated. In our series, MR clearly demonstrated the orbital abnormality in all but two cases; in several cases, MR appeared more sensitive than CT in providing additional information concerning the lesions. Much of the information added by MR was provided by its ability to directly produce images in the coronal and sagittal projections without additional positioning of the patient, affording excellent detail concerning alteration of the optic chiasm and optic nerve by pathologic masses. MR appeared to be more sensitive in detecting small areas of subacute and chronic hemorrhage within soft-tissue masses in the orbit, which may be important in management of the patient. In our patient with Kimura disease, the areas of hemorrhage within the orbital mass that were detected only with MR suggested that the mass had a very vascular nature. Biopsy demonstrated an extreme degree of angiogenesis associated with an inflammatory infiltrate, and subsequent therapy consisting of complete local surgical excision was instituted. Pathology confirmed areas of subacute and chronic hemorrhage in the highly vascular mass. On the other hand, as shown by DeLaPaz et al. [6], very recent hemorrhage may go undetected on MR since it may show signal intensity similar to normal brain tissue, and in these cases CT may be more sensitive. MR appears to be more sensitive than CT in detecting vascular ischemia of the globe, with signal intensity increasing in the vitreous as it undergoes liquefaction secondary to ischemia; as a result the vitreous has a long T2 relative to the normal vitreous.

Most of the tumors in our series showed long T1 and long T2 characteristics, with the general exception of melanomas and most meningiomas. The four melanomas in our series usually appeared to have relatively high signal on the T1-weighted images, in contrast to most other tumors, which had relatively long T1s. Increase in signal was noted in three of four melanomas on the T2-weighted images, while in one of the intraocular melanomas, there was low signal from the lesion. Since three of four melanomas showed a short T1 and long T2, unlike the effect of a paramagnetic substance such as melanin, they appear to be comparable to other subacute or chronic hemorrhagic tissue in signal characteristics. The one melanoma that demonstrated short T1 and short T2 did so most likely because of the paramagnetic effects of melanin. In all four cases of melanoma, CT showed a nonenhancing, hyperdense lesion that could have been interpreted as either tumor or hemorrhage. The meningiomas consisted of one optic-nerve-sheath meningioma and three sphenoid-wing meningiomas with extension into the orbit. In general, these showed low signal on both T1- and T2-weighted images, although all were detected with both MR and CT. The optic-nerve-sheath meningioma was in the apex of the right orbit and extended into the optic foramen; separation of the tumor from the optic nerve was not possible, as signal characteristics were similar. The optic-nerve glioma was confined to the intracranial optic nerve and chiasm, had long T1 and long T2 characteristics, and appeared slightly brighter on the T2-weighted images than the normal chiasm because of its long T2 characteristics. Our experience was similar to that of Daniels et al. [21] in that the optic-nerve gliomas and optic-nerve meningiomas produced relatively weak signals that made them difficult to distinguish from the normal optic nerve.

The other tumors in our series included two lymphomas, two metastatic adenocarcinomas, and three tumors extending directly into the orbit from adjacent paranasal sinuses, pathologically confirmed as mucoepidermoid carcinoma, squamous-cell carcinoma, and ossifying fibroma, all of which had both long T1 and long T2 characteristics. All of these mass lesions were detected with both MR and CT.

In our series, MR exhibited three limitations in imaging the orbit: (1) its inability to image calcifications within anatomic structures or in masses; (2) the lack of contrast discrimination between the high-signal retrobulbar fat and small hemorrhages with similar high signal intensity; and (3) the lack of contrast between the cortical bony margins of the orbit and adjacent air in the ethmoid and maxillary sinuses, which made

evaluation of the floor and medial wall of the orbit difficult, even though the lateral and superior walls of the orbit could be adequately examined due to good contrast between the bone and adjacent soft tissue or fat.

In conclusion, although MR still has limitations as compared with CT, it can provide additional information in examination of the orbit that may be important in early diagnosis. Further technical improvements, including surface coils [22, 23] applied close to the orbits and the availability of thinner sections [24, 25], will no doubt increase the information obtained.

REFERENCES

1. Bradley WG, Tosteson H. Basic physics of NMR. In: Kaufman L, Crooks LE, Margulis AR, eds. *Nuclear magnetic resonance imaging in medicine.* New York: Igaku-Shoin, **1981**:11–29
2. Crooks LE. Overview of NMR imaging techniques. In: Kaufman L, Crooks LE, Margulis AR, eds. *Nuclear magnetic resonance imaging in medicine.* New York: Igaku-Shoin, **1981**:30–52
3. Pykett IL, Newhouse JH, Buonanno FS, et al. Principles of nuclear magnetic resonance imaging. *Radiology* **1982**;143:157–168
4. Bradley WG, Newton TH, Crooks LE. Physical principles of nuclear magnetic resonance. In: Newton TH, Potts DG, eds. *Advanced imaging techniques.* San Anselmo, CA: Clavadel, **1983**:15–62
5. Hidayat AA, Cameron JD, Font RL, Zimmerman LE. Angiolymphoid hyperplasia with eosinophilia (Kimura's disease) of the orbit and ocular adnexa. *Am J Ophthalmol* **1983**;96:176–189
6. DeLaPaz RL, New PFJ, Buonanno FS, et al. NMR imaging of intracranial hemorrhage. *J Comput Assist Tomogr* **1984**;8:599–607
7. Wilner HI, Cohn EM, Kling G, et al. Computer assisted tomography in experimentally induced orbital pseudotumor. *J Comput Assist Tomogr* **1978**;2:431–435
8. Daniels DL, Haughton VM, Williams AL, Gager WE, Berns TF. Computed tomography of the optic chiasm. *Radiology* **1980**;137:123–127
9. Weinstein MA, Modic MT, Risius B, Duchesneau PM, Berlin AJ. Visualization of the arteries, veins, and nerves of the orbit by sector computed tomography. *Radiology* **1981**;138:83–87
10. Nugent RA, Rootman J, Robertson WD, Lapointe JS, Harrison PB. Acute orbital pseudotumors: classification and CT features. *AJNR* **1981**;2:431–436, *AJR* **1981**;137:957–962
11. Forbes GS, Earnest F IV, Waller RR. Computed tomography of orbital tumors, including late-generation scanning techniques. *Radiology* **1982**;142:387–394
12. Swenson SA, Forbes GS, Young BR, Campbell RJ. Radiological evaluation of tumors of the optic nerve. *AJNR* **1982**;3:319–326
13. Peyster RG, Hoover ED, Hershey BL, Haskin ME. Special article. High-resolution CT of lesions of the optic nerve. *AJNR* **1983**;4:169–174, *AJR* **1983**; 140:869–874
14. Bydder GM, Steiner RE, Young IR, et al. Clinical NMR imaging of the brain: 140 cases. *AJNR* **1982**;3:459–480, *AJR* **1982**;139:215–236
15. Brant-Zawadzki M, Davis PL, Crooks LE, et al. NMR demonstration of cerebral abnormalities: comparison with CT. *AJNR* **1983**;4:117–124, *AJR* **1983**;140:847–854
16. Sipponen JT, Kaste M, Ketonen L, Sepponen RE, Katevuo K, Sivula A. Serial nuclear magnetic resonance (NMR) imaging in patients with cerebral infarction. *J Comput Assist Tomogr* **1983**;7:585–589
17. Hawkes RC, Holland GN, Moore WS, Rizk S, Worthington BS, Kean DM. NMR imaging in the evaluation of orbital tumors. *AJNR* **1983**;4:254–256
18. Han JS, Benson JE, Bonstelle CT, Alfidi RJ, Kaufman B, Levine M. Magnetic resonance imaging of the orbit: a preliminary experience. *Radiology* **1984**;150:755–759
19. Sobel DF, Mills CM, Char D, et al. NMR of the normal and pathologic eye and orbit. *AJNR* **1984**;5:345–350.
20. Brant-Zawadzki M, Bartkowski HM, Ortendahl DA, et al. NMR in experimental cerebral edema: value of T1 and T2 calculations. *AJNR* **1984**;5:125–129.
21. Daniels DL, Herfkins R, Gager WE, et al. Magnetic resonance imaging of the optic nerves and chiasm. *Radiology* **1984**;152:79–83
22. Axel L. Surface coil magnetic resonance imaging. *J Comput Assist Tomogr* **1984**;8:381–384
23. Schenck JF, Wehrli FN, Charles HC, Zimmerman R, Norman D. Field dependence of contrast-to-noise in MR imaging of the brain. Presented at the annual meeting of the American Society of Neuroradiology, Boston, June **1984**
24. Hyman RA. Thin section imaging techniques. Presented at the Vanderbilt University MRI users meeting, Nashville, June **1984**
25. Crooks LE, Mills CM, Hoenninger JC, et al. Thin section MRI at 0.35 T. Presented at the annual meeting of the American Society of Neuroradiology, Boston, June **1984**